RESEARCH PAPER

The Effect of Different Heat Treatment Procedures on Duplex Stainless Steel Microstructures and Electrochemical Properties

M. Azadi*, M. Ferdosi and H. Shahin

* m.azadi@semnan.ac.ir

Received: May 2019 **Revised: August 2019** **Accepted: September 2019**

Faculty of Materials and Metallurgical Engineering, Semnan University, Semnan, Iran.

DOI: 10.22068/ijmse.17.1.91

Abstract: *In this paper, the effect of solutioning and various aging heat treatment processes on the microstructure, the hardness and electrochemical properties of a duplex stainless steel (DSS) were studied. The evaluation of the microstructure and phase compositions were carried out by the optical microscopy (OM) and the X-ray diffraction (XRD). Electrochemical behavior of specimens were evaluated by both potentiodynamic polarization and electrochemical impedance spectra (EIS) tests at 25 and 60 ºC. The obtained results showed that the solutioning heat treatment increased corrosion rates with respect to the blank specimen. The aging process at 490 ºC for 20 hrs increased the volume percent of the carbide phase to the highest value (25.1%) which resulted in an increase in the hardness value up to 170 VHN. The specimen which was aged at 540 ºC for 10 h with the Cr7C3 size of 22.8 µm, exhibited the higher corrosion resistance at both temperatures of 25 and 60 ºC with respect to other aged specimens. In addition, the temperature of 60 ºC promoted the anodic reactions in 3.5 wt.% NaCl solution which decreased impedance modulus values significantly. Consequently, the carbide size was more effective parameter than the carbide content in predicting electrochemical behavior of such alloys.*

Keywords: *Duplex Stainless Steel, Heat Treatment, Aging, Microstructure, Electrochemical Behaviors, Hardness.*

1. INTRODUCTION

Duplex stainless steels (DSSs) are known as high strength steels which have two phases of ferrite and austenite. Therefore, overall properties of such steels are depended on the volume fraction of each phase, the phase morphology, the grain size and the carbon content [1]. DSSs are widely applied in different applications such as petrochemical, gas and oil process industries [2, 3]. DSSs usually showed different behavior in the field of corrosion resistance and mechanical properties after aging heat treatments between 300 and 1000 °C. Such event is due to the formation of intermetallic phases, such as carbides, sigma, and chi phases, depending on the temperature and times of the aging process [4, 5]. Thus, there are many research which were done on aging heat treatments and their relation with steel properties. Straffelini et al. [5] studied the effect of aging process on the fracture behavior of lean DSSs with the low nickel content. They observed nitride phases after the aging process in the temperature range of 550 and 850 °C. Maetz et al. [6] used different analysis to provide a complete and accurate study of the precipitation occurring at the different interfaces in a 2101 lean DSS during the aging step at 690 °C. Li et al. [2] investigated the effect of aging process on the precipitation behavior and the pitting corrosion resistance of SAF2906 super DSS. The recommended temperature range was 600-1100 °C to increase corrosion resistance. Tawancy et al. [7] studied aging characteristics of a DSS for 1000 hrs at 315, 370, 425 and 480°C. They found that a nitride phase, with the chemical composition of $(Fe, Cr)_2N$, existed in the as-quenched sample. The aging process increased the volume fraction of that phase. Yinhui et al. [8] focused on the microstructure and the corrosion behavior for the aging step at 750 °C in 25% Cr DSS. They showed that in the early stage of aging at 750 °C up to 150 min, the retardation of σ-phase decreased the corrosion rate of the steel due to the higher solution treatment temperature. Wang et al. [9] demonstrated that the σ-phase was formed at 800-900 °C. The amount of σ-phase increased with the increase of time in the aging process. Badji et al. [10] reported that when the solution treatment temperature increased from 1050 to 1250 °C, the formation of

[DOI: 10.22068/ijmse.17.1.91]

the σ-phase was delayed, and increasing the aging temperature from 700 to 850 °C accelerated it. Garcia et al. [11] studied the corrosion behavior of DSS specimens made by the powder metallurgy process. Their results showed that the aging heat treatment at the temperature higher than 650 °C increased the corrosion resistance.

Although much work exists on the development of suitable alloy chemistry and heat treatments [1], there are interests on DSSs to achieve an optimum correlation of microstructural features with mechanical and electrochemical properties of such steels. Thus, in this article, the solutioning and various aging processes at the range of 490 to 540 ºC were done for a DSS. Then, hardness changes plus the electrochemical behavior of various specimens were investigated. In addition, microstructural evaluations were applied for better correlation between carbide phases and electrochemical behavior of DSSs.

2. MATERIAL AND METHODS

In this paper, specimens of a duplex stainless steels were used. The details of chemical composition of the material used is given in Table 1.

A solutioning process and various aging heat treatments were performed on specimens. Details of the procedures are reported in Table 2. For solutioning process, specimens were heated at 1050 °C for 1 hr [5] and then quenched in water to produce a homogenous mixture of austenite and ferrite microstructure. For aging process, specimens were aged at 490 and 540 °C for 10 to 20 hrs after solution step. It should be mentioned that the specimen without any heat treatment (blank sample) was used for the better comparison of the results.

After heat treatment process, specimens were polished up to 3000 grit papers and etched with Kalling's etchant. This etchant contained HCl, HNO_3, $CuCl_2$, $FeCl_3$, and methanol. The microstructure of various specimens was evaluated by optical microscopy (OM, Olympus model). Volume fractions and the mean size of carbide phases were determined by the Image J program. In addition, the presence of different phases in specimens were detected by X-ray diffraction (XRD, Bruker-D8 with Cu Kα anode) analysis. The X-ray angle (2θ) was in the range of 10-90° and the step angle was 0.06°. The hardness of all specimens was measured by a Vicker hardness tester. The applied force was 30 N. Three measurements were utilized to report the mean hardness value for each sample.

Table 1. The chemical composition of the utilized material

Fe	C	Cr	Ni	Mn	Mo	Nb	Cu
Bal.	0.24	18.790	8.600	1.820	0.473	0.250	0.208
	Si	W	V	Al	Ti	P	S
	0.197	0.164	0.104	0.047	0.039	0.027	0.016

Table 2. Utilized different heat treatment procedures

Specimen name	Solutioning temperature (°C)	Solutioning time (h)	Aging temperature (°C)	Aging time (h)
Quench	1050	1	-	-
490-10h	1050	1	490	10
490-20h	1050	1	490	20
540-10h	1050	1	540	10
540-20h	1050	1	540	20
Blank	-	-	-	-

[DOI: 10.22068/ijmse.17.1.91]

The electrochemical evaluation was carried out using potentiodynamic polarization tests. A three-electrode cell contained a platinum counter foil, the saturated calomel reference electrode (SCE) and the specimen. The scan rate was about 1 mV/s. Specimens with the surface area of 100 mm^2 were exposed to the corrosive environment. The corrosive environment was 3.5 wt% NaCl solution. The corrosion tests were perfumed at 25 and 60 °C. Moreover, electrochemical impedance spectra (EIS) experiments were conducted to evaluate the corrosion properties of specimens. The impedance data were collected at the frequency range between 100 kHz and 50 Hz. A sine wave with the amplitude of 10 mV was utilized.

3. RESULTS AND DISCUSSION

Fig. 1 shows OM images for all specimens. The microstructure of the blank specimen (Fig. 1a) consists of a matrix with alloy carbides. The matrix was a mixture of austenite and ferrite phases according to the Schaeffler diagram [12]. This diagram predicts that the utilized duplex phase steel should contain ferrite lower than 10% and the austenite phase higher than 90%. Such prediction was measured based on the nickel equivalent value of 9.96 and the chromium equivalent value of 19.68. By the solutioning process, large amounts of alloy carbides were solutionized in the matrix and only small amount with large size (black-colored

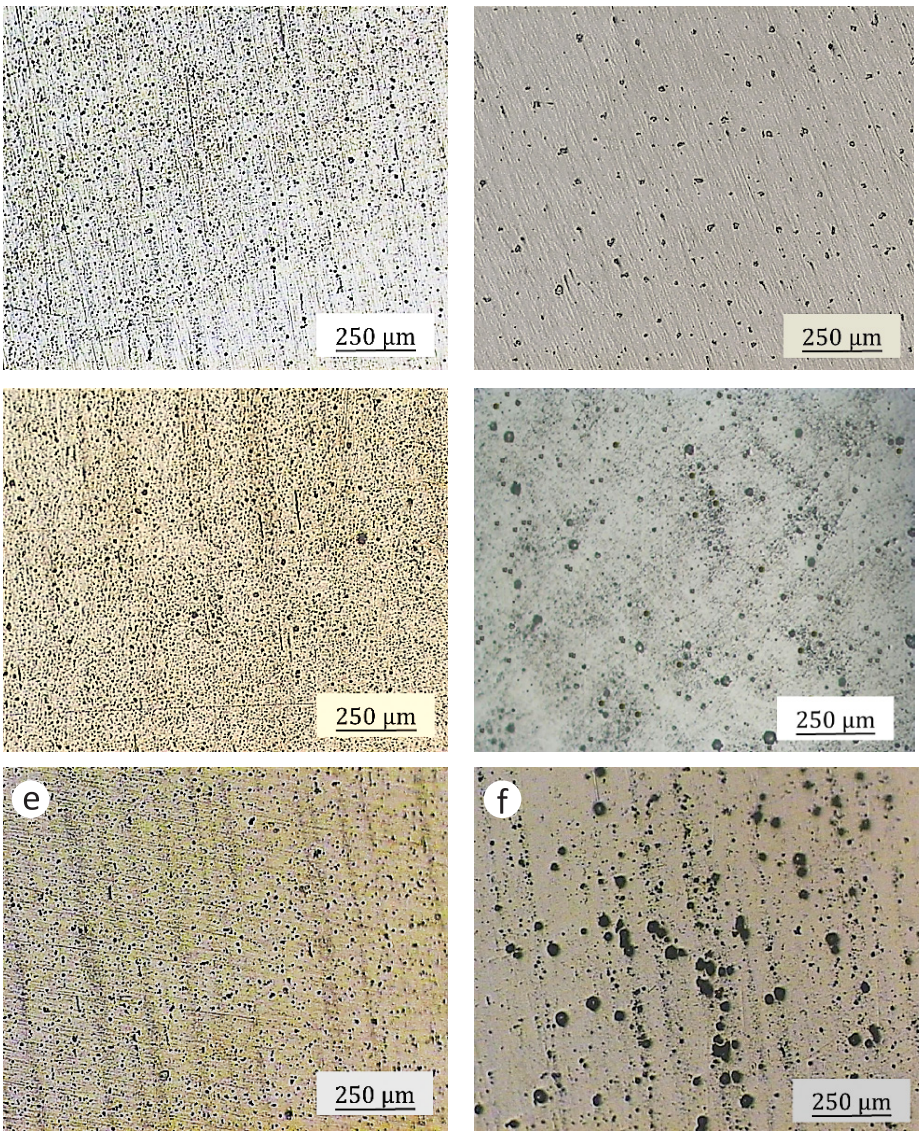

Fig. 1. OM images of various specimens showing alloy carbides distribution in the matrix including, (a) Blank, (b) Quench, (c) 490-10h, (d) 490-20h, (e) 540-10h and (f) 540-20h

[DOI: 10.22068/ijmse.17.1.91]

areas) retained in the matrix as shown in Fig. 1(b). Fig.1(c) shows that when the specimen was aged at 490 °C for 10 hrs after the solutioning process, the alloy carbides content in the matrix increased clearly. Such an event enhanced the hardness of the material. Increasing aging time to 20 hrs at the constant aging temperature of 490 °C, resulted in the coarsening of alloy carbides in some areas, as shown in Fig. 1(d). When the aging temperature changed from 490 to 540 °C, at the constant aging time of 10 hrs, the precipitation of alloy carbide in smaller size was observed (Fig. 1(e)). It was found that the highest precipitates growth occurred at the aging temperature of 490 °C [19]. However, by increasing the aging time at 540 °C from 10 to 20 hrs, the coarsening of alloy carbides was observed homogenously in more areas compared to 490 °C, as shown in Fig. 1(f). Microstructural parameters measurements from Image J program namely the volume percent and the mean size of alloy carbide are reported in Table 3. The solutioning process decreased the carbide volume from 16.4 to 3.8 % and the carbide size from 24.4 to 10.8 µm. The aging process at 490 ºC for 20 hrs increased the volume percent of carbide with the value of 25.1 However, the highest value of carbide size (48.2 µm) was related to the specimen which was aged at 540 ºC for 20 hrs. Therefore, the aging time was an effective parameter in enhancing the size of alloy carbide with respect to the alloy carbide content.

Vickers hardness test results for all specimens are seen in Fig. 2 (a). The initial mean hardness values for the blank specimen was about 153 VHN. The solutioning process decreased the hardness to 140 VHN due to the lowest alloy carbide content. The aging process at 490 °C for 20 hrs, increased the hardness to 170 VHN due to the highest content of carbides (Fig. 2 (b)). This result was similar to the report in the literature [13]. It was found that the best temperature for reaching the highest hardness was 482 °C for 4 hrs for specimens made by the powder metallurgy process. At the constant aging temperature of 490 °C, when the aging time increased from 10 to 20 hrs, the hardness value increased to 6% with respect to the lower time. In this situation, the increased in the carbide volume was 13% for the 490-20 specimen comparing with the 490-10 specimen. In addition, the coarsening alloy carbide at 540°C, increased the hardness value by 8% with respect to the lower time. Consequently, the alloy carbide content was an effective factor in enhancing the hardness in aged specimens.

Fig. 3 shows the XRD patterns for various specimens. For the blank specimen, without any heat treatment, the austenite phase was stable in (220), (111) and (200), while the ferrite phase was stable in planes of (110), (200) and (211), as shown in Fig. 3(a). Similar peaks were also reported in the literature [20]. The highest peak of the austenite phase was related to the plane of (220). Due to the higher intensity of the peaks related to austenite phase with respect to ferrite peaks, the amount of austenite phase was much higher than the ferritic phase. This results is in accordance with the Schaeffler diagram. The chemical composition of the alloy carbides was chromium carbide (Cr_7C_3) and the crystallographic structure was orthorhombic.

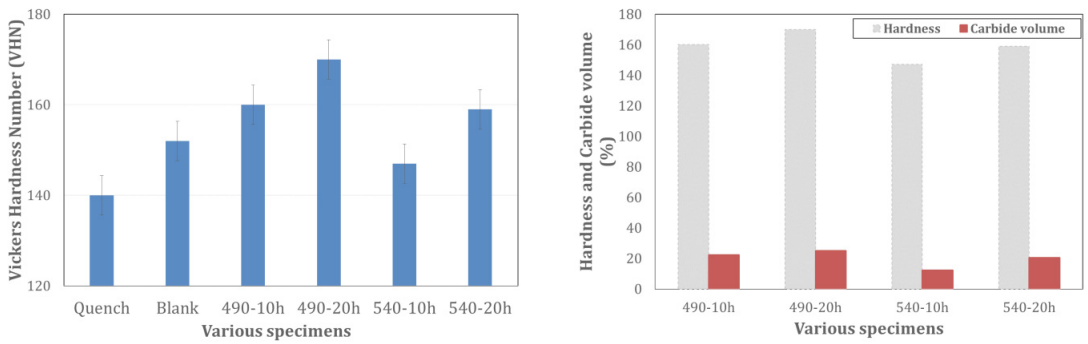

a b

Fig. 2. (a) Vickers hardness test results for all specimens and (b) Correlations of carbide volume with the hardness value for various aged specimens

[DOI: 10.22068/ijmse.17.1.91]

Table 3. Microstructural parameters measurements

Specimen	Volume percent of carbide phase (%)	Mean size of alloy carbide (μm)
Quench	3.8±1	10.8±5
490-10h	22.2±1	30.1±5
490-20h	25.1±1	40.4±5
540-10h	12.2±1	22.8±5
540-20h	20.5±1	48.2±5
Blank	16.4±1	24.4±5

When the specimen was solutionized at 1050 °C, the peak of alloy carbides disappeared in the XRD pattern (Fig. 3(b)). The latter observation is an indication that most of the chromium carbides were dissolved in the matrix. In addition, the most stable plane of austenite phase changed to (111). By applying the aging process, chromium carbides and ε-carbides with the chemical composition of Fe_2C precipitated in the matrix. The stability of the austenite phase was in planes of (220) and (111) (Fig. 3(c)). As shown in Fig. 3(d), with the increase in the aging temperature at lower aging time, the peak height of the carbide phase decreased. In addition, the highest peak of the austenite phase was related to the plane of (111). Such behavior affects the mechanical and corrosion behavior of used material. Additionally, the stability of the ferrite phase plane did not change significantly in all specimens. It can be stated that, the aging processes which resulted in the higher alloy carbide content changed the crystallographic features of the austenite phase. It was also seen

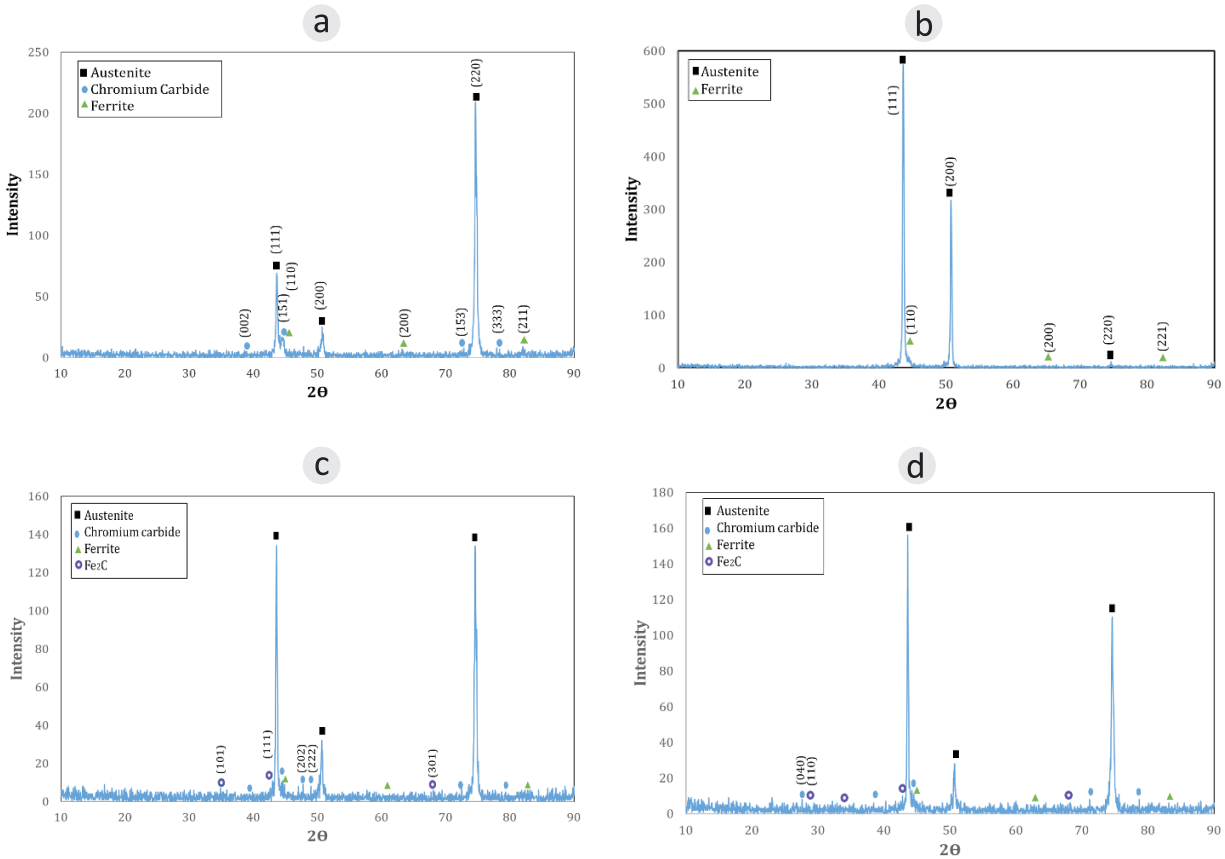

Fig. 3. XRD patterns for various specimens including, (a) blank, (b) Quench, (c) 490-20h and (d) 540-10h specimens

[DOI: 10.22068/ijmse.17.1.91]

that the sigma phase (σ-phase) is an intermetallic phase which contained mainly of iron and chromium and formed in ferritic and austenitic stainless steels during exposure at 540-980 °C when the chromium content was higher than 20 % [14-15]. Consequently, this phase did not appear in all specimens due to the low amount of chromium.

Fig. 4 depicts potentiodynamic polarization curves for various specimens in the 3.5 wt% solution of NaCl. To keep the stability of open-circuit potentials, all samples were immersed into the electrolyte for 30 mins.

As Table 4 shows the corrosion potential range was -230 to -420 mV at both temperatures. In addition, increasing the environment temperature raised the corrosion current. Such behavior was due to the increase in ionic transport and dissolution reactions in higher temperatures [18]. Additionally, the higher temperature of the corrosive environment increased the activity of chloride ions which promoted the corrosion rate [21]. The ratio of corrosion current at 60 ºC to corrosion current at 25 ºC for all specimens is measured and presented in Table 4. This ratio for all samples except for the quenched specimen was higher than the unity. This shows that the corrosion resistance was decreased at the higher temperature of the corrosive environment. At the temperature of 25 ºC, the quenched sample exhibited the highest corrosion rate with respect to other samples, as shown in Fig. 5. By increasing the temperature to 60 ºC, the 540-20h sample exhibited the highest corrosion rate. In addition, at both temperatures, the anodic passivity behavior for the utilized duplex stainless steel, which was the result of Cr_2O_3 formation, was not observed due to the presence of Cl^- ions in the corrosive solution. Increasing aging times rasied the corrosion current for both aging temperatures. A similar behavior was also showed by Luo et al. [19]. It should be pointed out that Cl^- ions are known to prevent the formation of the passive layer causing the pit initiation [20]; however, such an event did not observe for the used material.

To provide a more detailed discussion, the correlation between carbide size and corrosion current for various aged specimens for both temperatures is depicted in Fig. 6. It is shown that there was a direct relationship between the carbide size and the corrosion rate at both temperatures. In other words, the larger size of alloy carbide increased the corrosion current density. Such observation could be related to local microscopic anodic and cathodic regions on the metal surface, due to the presence of alloy carbides precipitates in the matrix. On the whole, the larger size of alloy carbide increased the surface inhomogeneity of the metal surface. Moreover, an unfavorable ratio of anodic to cathodic areas created with the coarsening of alloy carbides. At temperatures of 25 and 60 ºC, increasing the aging time from 10 to 20 h which was resulted in the increase of carbide size, decreased the corrosion resistance of the utilized alloy. It was noticed that there was not a significant relationship between the carbide volume and the corrosion rate. Consequently, the optimum carbide size for better corrosion resistance was about 22-24 µm. Additionally, the presence of

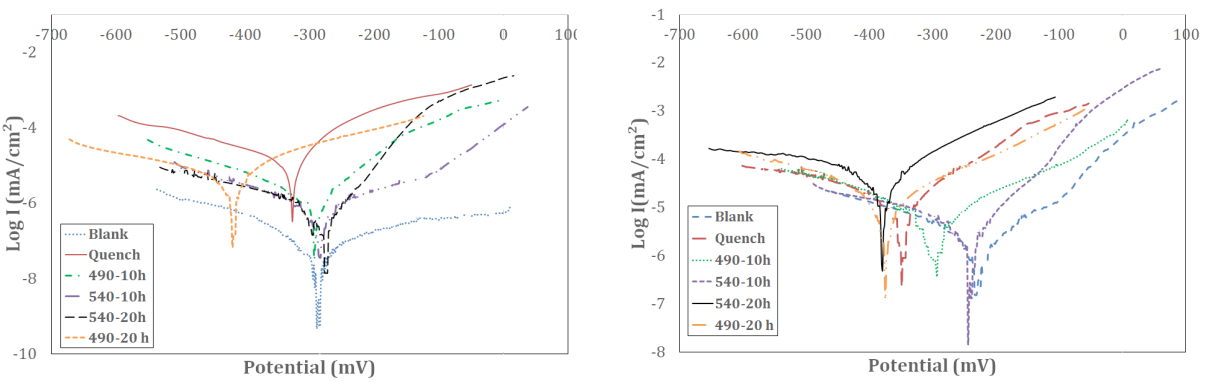

Fig. 4. Polarization test results for various specimens (obtained potential versus SCE potential), including (a) at 25 ºC and (b) 60 ºC

[DOI: 10.22068/ijmse.17.1.91]

Table 4. Corrosion currents and potentials for various specimens at 25 and 60 ºC

Specimen name	$I_{corr.}$ (mA/cm²)	$E_{corr.}$ (mV)	$I_{corr.}$ (mA/cm²)	$E_{corr.}$ (mV)	I_{60}/I_{25}
	at 25 ºC		at 60 ºC		
Quench	106.82	-315	10.13	-330	0.09
490-10h	1.61	-295	5.70	-300	3.27
490-20h	10.35	-420	11.86	-370	1.15
540-10h	0.81	-285	5.27	-250	7.04
540-20h	19.31	-280	62.60	-400	3.24
Blank	0.27	-290	3.70	-230	13.70

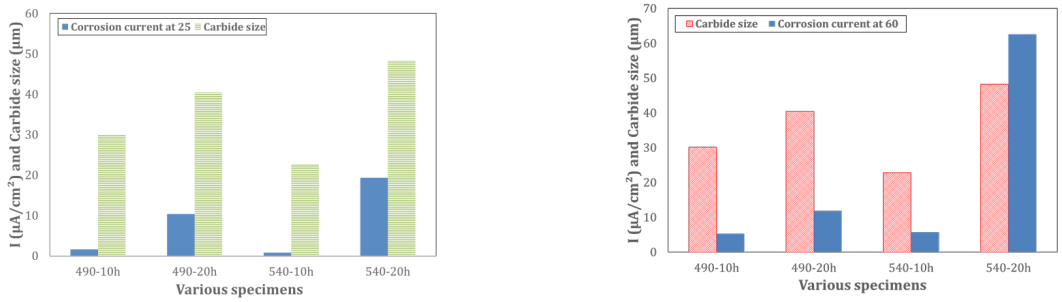

Fig. 5. Correlations of the carbide size with corrosion currents for various aged specimens including (a) at 25 ºC and (b) at 60 ºC

Fe_2C phase had an effective role in decreasing the corrosion resistance which precipitated in aged specimens compared to the blank specimen.

Polarization curves at higher potential range (-0.5 to 2 V with respect to SCE potential) at 25 ºC are shown in Fig. 6 to investigate the active-passive behavior. The anodic passivity of metals which was the result of the formation of Cr_2O_3 protective layer was observed in the voltages higher than 0 V for all specimens due to the presence of Cl^- ions in the corrosive environment. Similar results were reported by Loto et al. [20]. Additionally, the secondary passivation was also observed for the potentials higher than 0.75 V for all specimens, which could be related to the reaction of $Cr_2O_3 + 5H_2O = 2CrO_4^{2-} + 10H^+ + 6e$ [21]. Similar curves were also reported by Amador et al. [22].

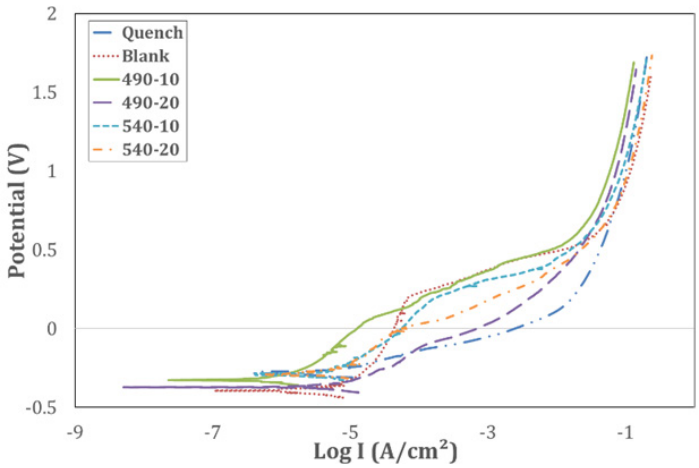

Fig. 6. Polarization test results for various specimens at 25 ºC at the higher applied potential range for showing the passive behavior

[DOI: 10.22068/ijmse.17.1.91]

Electrochemical characterization tests results are shown in Fig. 7. As shown in Fig. 7(a), which is known as bode plot, the impedance modulus for the blank sample decreased linearly at 25 ºC with increasing the frequency, although other specimens did not show such behavior. It was found that when the phase angle showed the lowest value in the low frequency, it was an indication for the creation of stable passive layer on the surface [17]. Thus, according to the results shown in Fig. 7 (b), the heat treatment processe created unstable films on surfaces of specimens. When the temperature of the corrosive environment increased from 25 to 60 ºC, the created film became thicker with higher porosities and led to the film rupture and a decrease the impedance

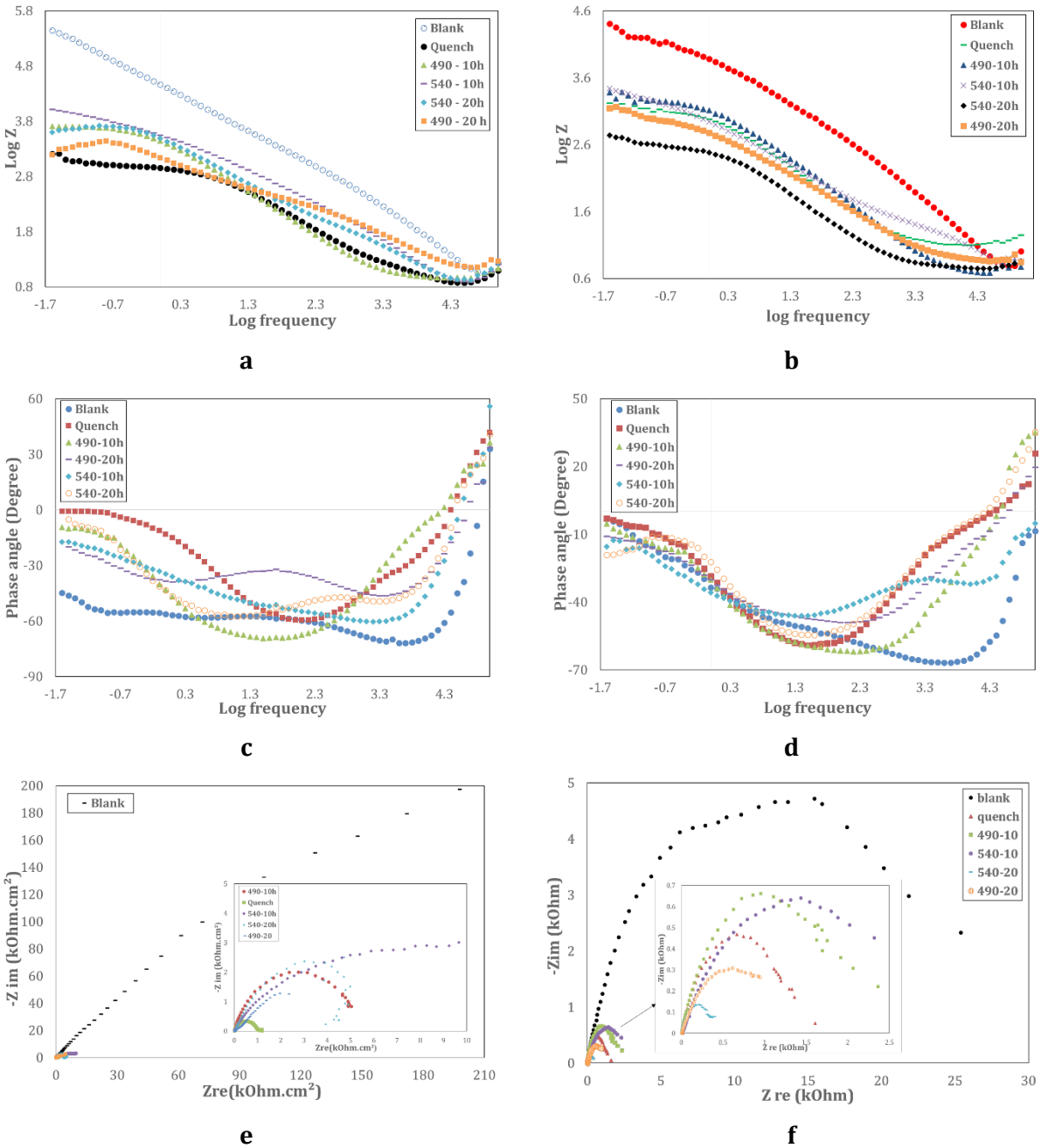

Fig. 7. (a) and (b) Bode plots for various samples in 3.5 wt% NaCl solution at 25 and 60 ºC, respectively, (b) and (d) phase angle plots for various specimens at 25 and 60 ºC, respectively and (e) and (f) Nyquist plots for various specimens at 25 and 60 ºC, respectively

[DOI: 10.22068/ijmse.17.1.91]

modulus. Such an observation has been reported previously. In bode plots, the impedance modulus decreased sharply by increasing frequency after the frequency of 1 Hz. Such behavior demonstrates the charge transfer mechanism on inhomogeneous surfaces [17].

Since the phase angle did not show the same high value of phase (close to 80 º) over a wide range of frequencies, it was found that unstable passive layers created on the surface of specimens at 60 ºC [24]. It was found that the presence of carbides phases could reduce the corrosion resistance of stainless steel [25]. In addition, Amador et al. [22] demonstrated that the metal dissolution was accelerated by exposing the steel surface at the temperature of 60 °C due to the breakdown of the passive layer. The best fit for the experimental measurements was done by the equivalent circuit model (as shown in Fig. 8) which contained three elements of the charge of the double-layer (CPE), the solution resistance (R_s) and the resistance of double-layer (R_p). Related parameters are reported in Table 5. Such equivalent circuit model was also represented for duplex stainless steels [17, 26-27].

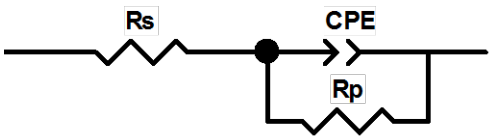

Fig. 8. The suggested equivalent circuit model

The range of R_s values at 25 ºC, was between 6.2 to 9.2 Ω. The highest and the lowest values of R_p for aged specimens were related to the 540-10h specimen and the 490-20h specimen, respectively. At the temperature of 60 ºC, R_p and R_s values decreased, while the value of CPE increased for aged specimens. A similar observation was also reported by the other research [18]. The decrease in R_p values indicated a reduction of the corrosion resistance of the adsorbed layer. Additionally, the rise in CPE values at 60 ºC showed that the thickness of the double layer which was the result of adsorption of water solution on the metallic surface decreased. In addition, such reduce in CPE values would be related to un-coverage of the charged surface by corrosion products [27]. On the whole, the higher capacitances of the double layer and the smaller polarization resistance decreased the corrosion resistance. It was noticed that the sum of R_s and R_p values attributed to the impedance modulus, at the low-frequency end in bode plots [26]. Thus, similar to the polarization test results, the 540-10h specimen had the highest corrosion resistance among other aged specimens at both temperatures. Consequently, changes in the type, volume and the size of carbides had a significant influence on the corrosion resistance of such alloys.

4. CONCLUSION

Duplex stainless steel microstructures have been developed to study the effects of the size and volume fraction of carbides on the hardness and electrochemical behaviors. The Main results of this study are summarized as follows:

1. The aging heat treatment increased the hardness values by 5 to 12% compared to the blank specimen when the specimen was aged at 540 and 490 ºC for 20 hrs, respectively.

Table 5. Equivalent electrical circuit parameters

Specimen	R_s (Ω)		CPE -T		CPE-P (n)		R_p (kΩ)	
	25 ºC	60 ºC	25 ºC ($F*10^{-5}$)	60 ºC ($F*10^{-4}$)	25 ºC	60 ºC	25 ºC	60 ºC
Quench	7.8	6.5	7.3	1.4	0.90	0.89	1.4	1.8
490-10h	8.7	5.9	5.6	1.2	0.93	0.85	5.3	2.2
490-20h	6.4	5.0	10.1	3.6	0.91	0.88	3.3	1.3
540-10h	9.2	8.1	4.3	3.4	0.95	0.91	9.8	3.1
540-20h	6.2	5.4	6.2	4.2	0.91	0.89	6.6	0.4
Blank	9.1	7.1	1.0	0.3	0.85	0.83	36.4	17.6

[DOI: 10.22068/ijmse.17.1.91]

2. The solutioning heat treatment decreased the hardness value from 152 to 140 VHN and lowered the corrosion resistance at 25 ºC compared with the blank specimen due to the decrease of the size of alloy carbides in the austenite matrix.
3. When the specimen aged at 540 ºC for 10 hrs, the highest corrosion resistance was achieved among aged specimens due to the lower size of alloy carbides precipitated in the matrix.
4. Both EIS and polarization tests results showed that the higher carbide content and the larger size of alloy carbides increased the corrosion rate for both temperatures of 25 and 60 ºC. This behaviour was related to specimens which were aged at 490 ºC.
5. The presence of Fe_2C phase in aged samples increased the corrosion rate in 3.5 wt% NaCl solution. In addition, the optimum size of alloy carbides with the value of 20-22 µm was an effective parameter to lower the corrosion rate in such duplex stainless steel.
6. Corrosion tests results demonstrated that the higher temperature with the value of 60 ºC in corrosion measurement tests promoted corrosion rates of all specimens except for the quenched specimen.

REFERENCES

1. Chakraborti, P. C. and Mitra, M. K., "Microstructure and tensile properties of high strength duplex ferrite–martensite (DFM) steels", Mater. Sci. Eng. A. 2007, 466, 123-133.
2. Li, J., Li, G., Liang, W., Han, P. and Wang, H., "Effect of aging on precipitation behavior and pitting corrosion resistance of SAF2906 super duplex stainless steel". J. Mater. Eng. Perform., 2017, 26, 4533-4543.
3. Liang, T., Hu, X., Kang, X. and Li, D., "Microstructure evolution of a cold-rolled 25Cr-7Ni-3Mo-0.2N duplex stainless steel during two-step aging treatments". Acta Metallurgica Sinica, 2013, 26, 517-522.
4. Silva, R., Baroni, L. F. S., Silva, M. B. R., Afonso, C. R. M., Kuri, S. E. and Rovere, C. A. D., "Effect of thermal aging at 475 °C on the properties of lean duplex stainless steel 2101". Mater. Character., 2016, 114, 211-217.
5. Straffelini, G., Baldo, S., Calliari, I. and Ramous, E., "Effect of aging on the fracture behavior of lean duplex stainless steels". Met. Mater. Trans. A, 2009, 40, 2616- 2622.
6. Maetz, J. Y., Douillard, T., Cazottes, S., Verdu, C. and Kleber, X., "$M_{23}C_6$ carbides and Cr_2N nitrides in aged duplex stainless steel: A SEM, TEM and FIB tomography investigation", Micron, 2016, 84, 43-53.
7. Tawancy, H. M. and Abbas, N. M., "Ageing characteristics of a duplex stainless steel". J. Mater. Sci. Lett., 1988, 7, 676-678.
8. Yinhui, Y., Biao, Y., Junlin, Y., Yuxin, W. and Gang, D., "Microstructure and corrosion behavior aging at 750 °C in 25% Cr duplex stainless steel". Rare Metals, 2011, 30, 515-520.
9. Wang, X. F., Chen, W. Q. and Zheng, H. G., "Influence of isothermal aging on σ precipitation in super duplex stainless steel". Int. J. Min. Met. Mater., 2010, 17, 435-441.
10. Badji, R., Kherrouba, N., Mehdi, B., Cheniti, B., Bouabdallah, M., Kahloun, C. and Bacroix, B., "Precipitation kinetics and mechanical behavior in a solution treated and aged dual phase stainless steel". Mater. Chem. Phys., 2014, 148, 664-672.
11. Garcia, C., Martin, F., Blanco, Y. and Aparicio, M. L., "Effect of ageing heat treatments on the microstructure and intergranular corrosion of powder metallurgy duplex stainless steels". Corr. Sci., 2010, 52, 3725–3737.
12. Guiraldenq, P. and Duparc, O. H., "The genesis of the Schaeffler diagram in the history of stainless steel". Met. Res. Technol., 2017,114, 613-620
13. Schade, C., Stears, P., Lawley, A. and Doherty, R., "Precipitation hardening P/M stainless steels". Int. J. Pow. Met., 2007, 43, 60-64.
14. Azadi, M., Pazuki A. M. and Olya, M. J., "The Effect of New Double Solution Heat Treatment on the High Manganese Hadfield Steel Properties". Met., Microstructure, Analysis, 2018, 7, 618-626
15. Hsieh, C. C. and Wu, W., "Overview of intermetallic sigma (σ) phase precipitation in stainless steels". Int. Scholarly Res. Notices Met., 2012, 2012, 732-471.
16. Jinlong, L., Tongxiang, L., Chen, W. and Limin, D., "Effect of ultrafine grain on tensile behavior

[DOI: 10.22068/ijmse.17.1.91]

and corrosion resistance of the duplex stainless steel". Mater. Sci. Eng. C, 2016, 62, 558-563.
17. Luo, H., Dong, C. F., Cheng, X. Q., Xiao, K., Li and X. G., "Electrochemical behavior of 2205 duplex stainless steel in NaCl solution with different chromate contents". J. Mater. Eng. Perform. 2012, 21, 1283-1291.
18. Dong, C., Luo, H., Xiao, K., Sun, T., Liu, Q. and Li, X., "Effect of temperature and Cl^- concentration on pitting of 2205 duplex stainless steel". J Wuhan Univ. Technol. Mater. Sci. Ed., 2011, 26, 641-649.
19. Luo, H., Yu, Q., Donga, C., Shad, G., Liu, Z., Liang, J. , Wang, L., Han, G. and Li, X., "Influence of the aging time on the microstructure and electrochemical behavior of a 15-5PH ultra-high strength stainless steel". Corr. Sci., 2018, 139, 185-196.
20. Loto, R. T., "Electrochemical corrosion characteristics of 439 ferritic, 301 austenitic, S32101 duplex and 420 martensitic stainless steel in sulfuric Acid/NaCl Solution", J. Bio Tribo Corr., 2017, 3, 24-32.
21. Li, H., Jiang, Z., Feng, H., Wang, Q., Zhang, W., Fan, G., Li, G. and Wang, L., "Electrochemical corrosion characteristics of super duplex stainless steel S32750 in LT-MED environment". Int. J. Electroch. Sci., 2015, 10, 1616-1631.
22. Amador, A. S., T. Ramirez, J. E., Castro, D. Y. V., Nunez, J. R. C., E. Duran, H. A. and Ballesteros, D. Y. P., "Electrochemical behavior of stainless steel AISI 430 exposed to simulated food". Revista Mater., 2018, 23, 1-8.
23. Elhoud, A. M., Renton, N. C. and Deans, W. F., "The effect of manufacturing variables on the corrosion resistance of a super duplex stainless steel". Int. J. Adv. Manufac. Technol., 2011, 52, 451-461.
24. Makhdoom, M. A., Ahmad, A., Kamran, M., Abid, K. and Haider, W., "Microstructural and electrochemical behavior of 2205 duplex stainless steel weldments". Surf. Inter, 2017, 9, 189-195.
25. Pezzato, L., Lago, M., Brunelli, K., Breda, M. and Calliari, I., "Effect of the heat treatment on the corrosion resistance of duplex stainless steels". J. Mater. Eng. Perform., 2018, 27, 3859-3868.
26. Cheng, T. P., Tsai, W. T. and Lee, J. T., "Electrochemical and corrosion behavior of duplex stainless steels in Hank's solution". J. Mater. Sci., 1990, 25, 936-943.
27. Sherif, E. S. M., "Corrosion behavior of duplex stainless steel alloy cathodically modified with minor ruthenium additions in concentrated sulfuric acid solutions". Int. J. Electroch. Sci., 2011, 6, 2284-2298.

[DOI: 10.22068/ijmse.17.1.91]